Bull. Astr. Soc. India (2014) **42**, 27–37

Possible detection of a cool-core in the cluster RXC J1252.5–3116

Kiran Lakhchaura * and K. P. Singh
Tata Institute of Fundamental Research, 1 Homi Bhabha Road, Colaba, Mumbai 400 005, India

Received 2014 February 3; accepted 2014 April 21

Abstract. This paper presents a detailed study of X-ray emission from the cluster RXC J1252.5–3116, based on an analysis of the *Chandra* archival data. Here we present radial profiles and maps of X-ray surface-brightness, temperature, electron number density, entropy and pressure of RXC J1252.5–3116. We have also estimated the X-ray luminosity, gas mass, cooling time and mass deposition rate for the cluster. The cluster shows an extremely relaxed X-ray morphology and the radial profiles suggest a drop in the temperature of the central gas. We find an extremely small cool-core and a high mass deposition rate of 43 $M_\odot$ per year. RXC J1252.5–3116 seems to host a possible cool core at its centre.

Keywords : galaxies: clusters: general – galaxies: clusters: individual:(RXC J1252.5–3116) – galaxies: clusters: intracluster medium — X-rays: galaxies: clusters

1. Introduction

Clusters of galaxies are the perfect systems for studying the various physical processes related to structure formation in the universe. Technological advancements in the field of X-ray astronomy during the last four decades have brought in a great wealth of information and have enormously improved our understanding of the physics of clusters, and have led to the detection of a large number of clusters, which were previously undetected in the optical. All sky and dedicated surveys done with these observatories have provided large statistically complete samples of clusters that have greatly improved our understanding of the general properties of clusters and their cosmological implications. Follow-up observations of some of the newly detected clusters with more advanced high-resolution X-ray observatories have enabled detailed studies of individual clusters.

*email: kiran_astro@tifr.res.in

Clusters of galaxies, in general, have highly peaked X-ray surface-brightness distributions, which are explained by the phenomenon of 'Cooling flows'. These flows are constituted when the rapidly cooling gas near the central parts of the cluster moves towards the centre due to the pressure exerted by the overlying hotter gas layers (see Fabian 1994, for a review). This simple homogeneous model of cooling flows, however, does not explain many of the observations. A huge discrepancy was observed in the amount of cooled gas expected from the peaked X-ray surface-brightness distributions and that confirmed from the spectroscopic observations. This was later explained by invoking various heating mechanisms. Recent high-resolution X-ray and low-frequency radio observations of clusters have revealed that the energy released in the central active galactic nuclei (AGN) outbursts can provide the expected amount of heating (see Fabian 2012, for a review). X-ray observations also disprove the homogeneous nature of cooling flows, suggested in the initial model. The spatial distributions of the cool-cores of clusters (up to a few hundreds of kpc) demand inhomogeneity in the cooling flows. The X-ray surface-brightness profiles and spectra of clusters with strong cooling flows often require multi-component fits, pointing towards the requirement of multiphase models (see Fabian 1994; Fukazawa et al. 1994; Peres et al. 1998; Gu et al. 2012). Although high-resolution *Chandra* X-ray observations of cool core clusters have provided some insights into this subject, more number of deeper X-ray observations of individual cool-core clusters are required for a better understanding of the spatial distribution and composition of the cooling flows.

In this paper we present our analysis of the archival data from a *Chandra* observation of the cluster RXC J1252.5–3116, which is found to be a possible cool-core cluster, in our analysis. The cluster is located in the Shapley Supercluster (deFilippis, Schindler & Erben 2005) and was first detected in the *ROSAT* All Sky survey (Pierre et al. 1994). The position and redshift of the cluster, and details of the *Chandra* observation used in this paper are given in Table 1.

Here, we present the X-ray and optical morphologies, the global spectral parameters, projected radial profiles and maps of thermodynamic quantities of the cluster. The details of the data reduction and the analysis are given in §2, and a summary of the results has been given in §3. Reid (2000) found a radio source coinciding with the brightest cluster galaxy from the National Radio Astronomy Observatory (NRAO) Very Large Array (VLA) Sky Survey (NVSS) image of the cluster. However, since the radio source was very weak (Reid 2000), we have not analyzed the radio observations of the cluster here. A lambda cold dark matter cosmology with H_0 = 70 km s^{-1} Mpc^{-1} and Ω_M = 0.3 (Ω_Λ = 0.7) has been assumed throughout.

Table 1. Redshift (z) and positions (α (J2000), δ (J2000)) of RXC J1252.5–3116 along with the details (observation ID, date of observations ad exposure time) of the *Chandra* observation used here.

z	α (J2000)	δ (J2000)	Obsn. ID	Date of Observation	Exposure Time (ks)
0.0535	12 52 33.6	-31 16 16	12275	2011 mar 20	10.1

2. Data analysis and results

The CIAO version 4.3 and CALDB version 4.4.0 have been used for analyzing the data. The data were reprocessed using the standard *chandra_repro* tool to produce the level 2 reduced event files (evt2) from the level 1 event files (evt1).

2.1 X-ray and optical morphology

The ciao task *dmcopy* was used to create an image of the cluster in the energy range of 0.3 to 8.0 keV. The binning factor was set to 8 (pixel size$\sim$ 4.0″). The ciao task *wavdetect* was used for detecting point sources in the image. A total of 23 sources were detected and were then removed from both image as well as event files. The ciao task *dmfilth* was used to fill the holes created in the image after point source removal. Gaussian kernels of width 4″ was used for smoothing the image and the ciao task *aconvolve* was used for this purpose. As a final step we created an exposure map for the cluster which was used to normalize the X-ray image. The exposure-corrected, point source removed and smoothed X-ray image of RXC J1252.5–3116 is shown in the left-hand-side of Fig. 1. The right-hand-side of Fig. 1 shows an overlay of the X-ray intensity contours on the optical image of the cluster from the SuperCOSMOS survey in the B_J band. RXC J1252.5–3116 seems to have a spherically symmetric X-ray morphology.

We have also created a radial profile of X-ray surface brightness of the cluster, using 56 circular annuli of width 4″ each. Both single-β ($S(r)= S_{01}(1 + (r/r_{c1})^2)^{-3\beta+0.5}$) and double-$\beta$ ($S(r)= S_{01}(1 + (r/r_{c1})^2)^{-3\beta+0.5} + S_{02}(1 + (r/r_{c2})^2)^{-3\beta+0.5}$) models were used for fitting the profile. Here, S(r) denotes the total surface-brightness at distance r from the cluster centre; S_{0i} and r_{ci} are the peak surface-brightness and core radius of the i^{th} model component (i=1 for single-β model and i=1,2 for double-β model), and β is the β-index. The fit obtained by using the double-β model was much better than that with the single-β model (F-test confidence level > 95%). The minimum value of the reduced chi-square ($(\chi^2_\nu)_{min}$ for the double-β model fit reduced to 0.55 from a value of 1.3 obtained for the single-β model. Fig. 2 shows the X-ray surface brightness profile of the cluster, fitted with the double-beta model (dashed line). The parameters obtained from the double-β model fit i.e. S_{01}, S_{02}, r_{c1} ,r_{c2} and β, are given in Table 2. The core radius of the smaller component of the double-β model (r_{c1}) for RXC J1252.5–3116 is found to be extremely small (=14±3 kpc), suggesting the presence of a possible cool core at the centre (see Eckert, Molendi & Paltani 2011; Hudson et al. 2010).

2.2 Average X-ray spectral analysis

We have used the X-ray spectral fitting package *Xspec* (version 12.7.0) for all the spectral analyses done in this paper. Using the point source removed event file, an average spectrum for the cluster was created in the energy band of 0.5-7.0 keV. A circular region of size 196″ centred on the peak of the surface-brightness of the cluster, was used for this purpose. The plasma emission

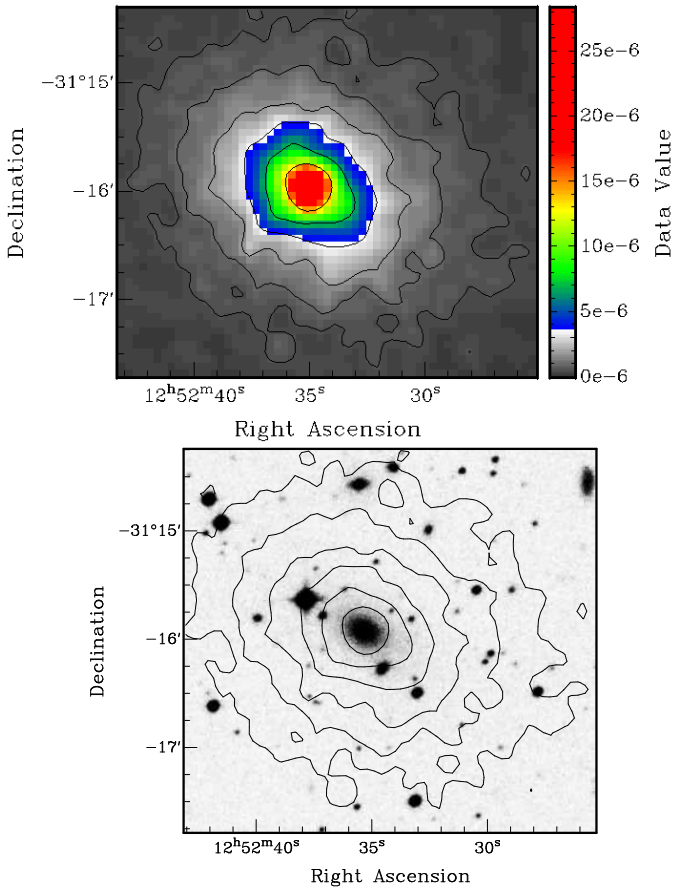

Figure 1. Top : *Chandra* X-ray image of the cluster RXC J1252.5–3116, smoothed with a Gaussian kernel of width 4″. The contours levels are logarithmically distributed between 10σ to 314σ above the mean background, from the outermost to the innermost contour. The scale is expressed in units of cts s^{-1} cm^{-2} $pixel^{-1}$. Bottom : Optical image of the cluster from the SuperCOSMOS survey overlaid with the X-ray contours.

model *apec* (Smith et al. 2001) along with the *wabs* photoelectric absorption model (Morrison & McCammon 1983), was used for the spectral fitting. The value of the neutral hydrogen column density along the line of sight to the cluster and the redshift of the cluster were frozen to the values obtained from the Leiden/Argentine/Bonn (LAB) Galactic HI survey (Kalberla et al. 2005) and the SIMBAD astronomical database, respectively. Figure 3 shows the average spectrum along with the histogram of the best fit model. The best fit values of the temperature, abundance and *apec* normalization obtained from the fit are given in Table 3. We also tried fitting the spectrum with a two-temperature model and a cooling- flow model, separately, but due to poor statistics, no

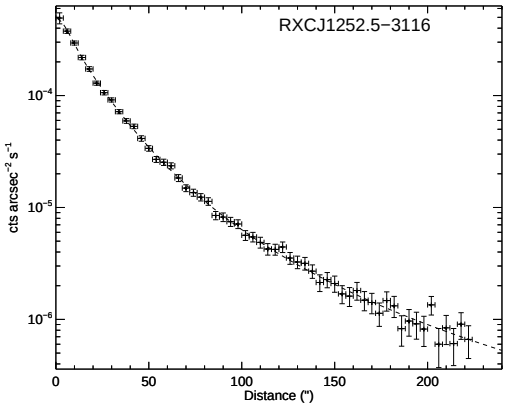

Figure 2. X-ray surface brightness profiles of the cluster RXC J1252.5–3116 fitted with a double-beta model, shown with the dashed line. The results of the fitting are provided in Table 2.

Table 2. Results obtained from the double-beta model fitting of the X-ray surface brightness profiles of RXC J1252.5–3116 as described in §2.1. Here, S_{01} and S_{02} are the peak surface brightness, r_{c1} and r_{c2} are the corresponding core radii, and β is the beta-index (assumed same for both the components) of the two components of the double-β model. The minimum reduced chi-square ($(\chi^2)_\nu$ and the degrees of freedom (DOF) obtained from the fit are also given.

S^*_{01}	S^*_{02}	r_{c1} (kpc)	r_{c2} (kpc)	β (= $\beta 1 = \beta 2$)	$(\chi^2_\nu)_{\rm min}$ (DOF)
31.1±3.3	17.5±3.9	14±3	34±4	0.66±0.02	0.55 (51)

All errors are quoted at 90% confidence level based on χ^2_{min}+2.71.
* S_{01} and S_{02} are expressed in the units of 10^{-5} counts s^{-1} arcsec^{-2}

significant improvement was seen in the results and the resultant parameters were found to have large errors.

Background subtraction for spectra : During the spectral fitting of the average spectrum, the local background subtraction was found insufficient to remove the particle and cosmic background components, and led to large residuals towards the high-energy-end of the spectrum. Additionally, X-ray emission from the cluster was detected from almost the entire detector, and it was impossible to find local emission-free regions. To overcome these problems, we used the *Chandra* blank-sky background observations for creating background spectra for all the spectral analyses done in this paper.

We have also estimated the X-ray luminosity (L_X in the energy range 0.5-7.0 keV) and the bolometric X-ray luminosity (L_X^{bol} in the energy range 0.1-100 keV) for the cluster. Both the values are given in Table 4. The L_X^{bol} value has been corrected for the small field of view of the

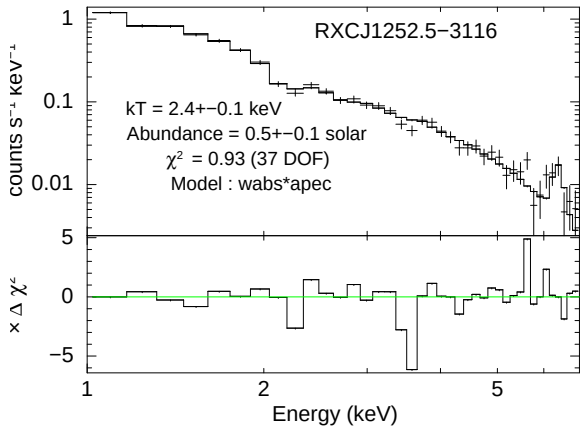

Figure 3. Average spectrum of the cluster RXC J1252.5–3116 from the *Chandra ACIS* detector. The spectrum has been fitted with *wabs*apec* model shown as a histogram. Details of the spectral analysis are given in §2.2, and the best-fit parameters are shown here in an inset.

detector by scaling it up to a radius of 1 Mpc, using the results of the double β-model fit obtained in §2.1.

Table 3. Average spectral properties of RXC J1252.5–3116 obtained from the analysis described in §2.2.

kT (keV)	Abundance (Rel. to solar)	*apec* norm. (10^{-3} cm^{-5})	$(\chi^2_\nu)_{min}$ (DOF)
2.4 ± 0.1	0.5 ± 0.1	12.6 ± 0.8	0.93 (37)

All errors are quoted at 90% confidence level based on χ^2_{min}+2.71.

2.3 Radial profiles of thermodynamic quantities : cooling time and gas mass

We have produced azimuthally averaged profiles of various thermodynamical quantities viz. temperature (kT), electron density (n_e), entropy (S), and pressure (P) for RXC J1252.5–3116. For this purpose we extracted and analyzed spectra in the energy band of 0.5 to 7.0 keV from 8 circular annuli centred on the X-ray emission peak of the cluster. The width of each annulus was fixed such that it has sufficient (≥600) counts in it. The details of the spectral analyses performed were same as given in §2.2, except that here the elemental abundance for all the annuli was frozen to the average abundance value (0.5 times solar; see Table 3) obtained for the cluster. As projection effects tend to smooth out the spatial variations of the thermodynamic quantities, we also carried out a deprojection analysis of the annuli spectra for each cluster, using the techniques described in Ehlert et al. (2011). All the projected (red) and deprojected (blue) profiles, thus obtained, are shown in Fig. 4. The temperature profiles were obtained as a direct result of the spectral analyses and are shown as the top left sub-figure. The electron density (n_e), entropy (S), and pressure

profiles were obtained by using the method described in Lakhchaura et al. (2011, 2013), and are shown as the top right, bottom left and bottom right sub-figures.

The projected and deprojected profiles of temperature are found to have large errors. On an average the temperature seems to increase with radius (except in the outermost annulus where it drops). We tried fitting a linearly increasing as well as a constant models to both projected and deprojected temperature profiles. Using the F-statistic, we found a slight improvement (probability ∼94.12% for projected temperature profile and ∼95.08% for deprojected temperature profile) with the linearly increasing model fit as compared to the constant model fit. The innermost annulus shows a slight increase in the temperature at the centre. The temperature profile suggests that cluster hosts a possible cool-core at its centre. The projected as well as deprojected density, entropy and pressure profiles of the cluster show an average decrease, increase, and decrease, respectively, from the centre outwards.

We have also calculated the central cooling time of the cluster. For this purpose, we used the gas temperature and density of the innermost annulus obtained in the deprojection analysis, and the following equations from Sarazin (1988) :

$$t_{cool} = 8.5 \times 10^{10} \mathrm{yr} \left[\frac{n}{10^{-3} \mathrm{cm}^{-3}} \right]^{-1} \left[\frac{T_g}{10^8 \mathrm{K}} \right]^{1/2} \quad (1)$$

The central cooling time of $(1.8 \pm 0.3) \times 10^9$y is found to be less than the Hubble time, and therefore, the cluster seems to be a possible cool-core-cluster. A profile of the cooling times obtained by using the full deprojected gas temperature and density profiles is shown in Fig. 5. The cooling radius, r_{cool} i.e. radius at which the cooling time is equal to 7.7 Gyr (marked using a vertical dotted line in Fig. 5, is found to be ∼67″ (∼ 70 kpc).

We fitted the projected density profile of the cluster with a single β-model i.e.,

$$n_e(r) = n_e(0) \left(1 + \frac{r^2}{r_c^2} \right)^{(3/2)\beta}, \quad (2)$$

where $n_e(0)$ is the central density and r_c is the core radius. Using the fit results and the following formula from Donnelly et al. (2001), we estimated the gas mass ($M_{gas}(r)$) of the cluster out to radius of 1 Mpc.

$$M_{gas}(r) = 4\pi\rho_0 \int_0^r s^2 \left[1 + \left(\frac{s}{r_c} \right)^2 \right]^{(3/2)\beta} ds \quad (3)$$

$\rho_0 = \mu n_e(0) m_p$; m_p is the mass of a proton and μ is the average molecular weight for a fully ionized gas (=0.609 from Gu et al. 2010). The value of the gas mass obtained for the cluster is given in Table 4.

We have also estimated the classical mass deposition rate for the cluster, $\dot{M}_{classical}$, within r_{cool}, using the formula given in Hudson et al. (2010) i.e. $\dot{M}_{classical}(< r) = M_{gas}(r)/(t_{cool}(r) - t_{cool}(0)$. The value was found to be 43 solar masses per year, which is in agreement with the values generally observed for the cool-core clusters (see Hudson et al. 2010).

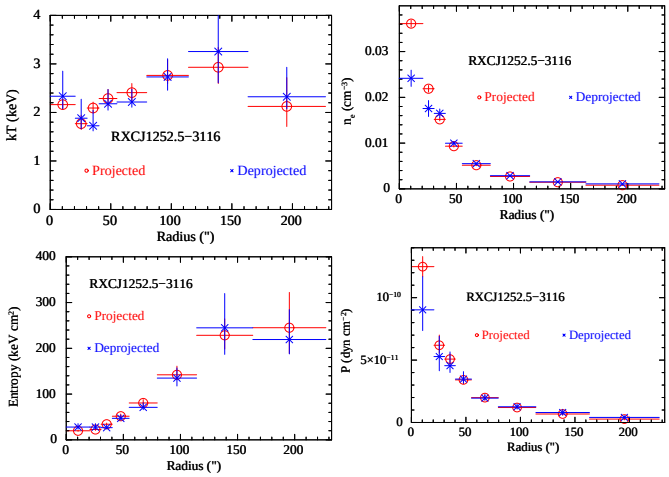

Figure 4. Profiles of projected (red) and deprojected (blue) temperature (kT), density (n_e), entropy (S) and pressure (P) obtained from the spectral analysis of circular annuli centred on the surface brightness peaks of the cluster RXC J1252.5–3116. The value of elemental abundance was frozen to the avearge abundance obtained for the whole cluster.

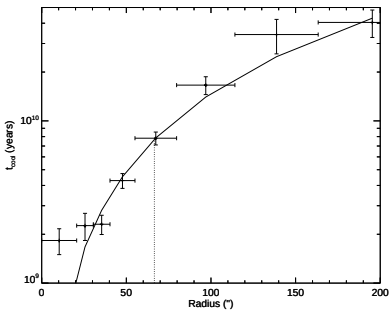

Figure 5. Cooling time of the cluster calculated at different radii. The cooling radius (r_{cool}) has been marked using a dotted line. The solid line shows a power-law fitted to the profile.

2.4 2D-projected thermodynamic maps

To look for non-isotropic (if any) and better resolved spatial variations of thermodynamic quantities, we have also produced projected temperature (kT), abundance, density (n_e), entropy (S), and pressure (P) maps of RXC J1252.5–3116. For this purpose we analyzed spectra from 21 box-shaped regions. All these spectra were extracted in the energy range of 0.5-7.0 keV. The sizes of the boxes were chosen carefully so that each of them has sufficient (≥600) counts in it. Smaller sized boxes were chosen in the inner brighter parts of the cluster and larger sized boxes were chosen in the outer fainter parts. Details of the spectral fitting, and the relations used to calculate

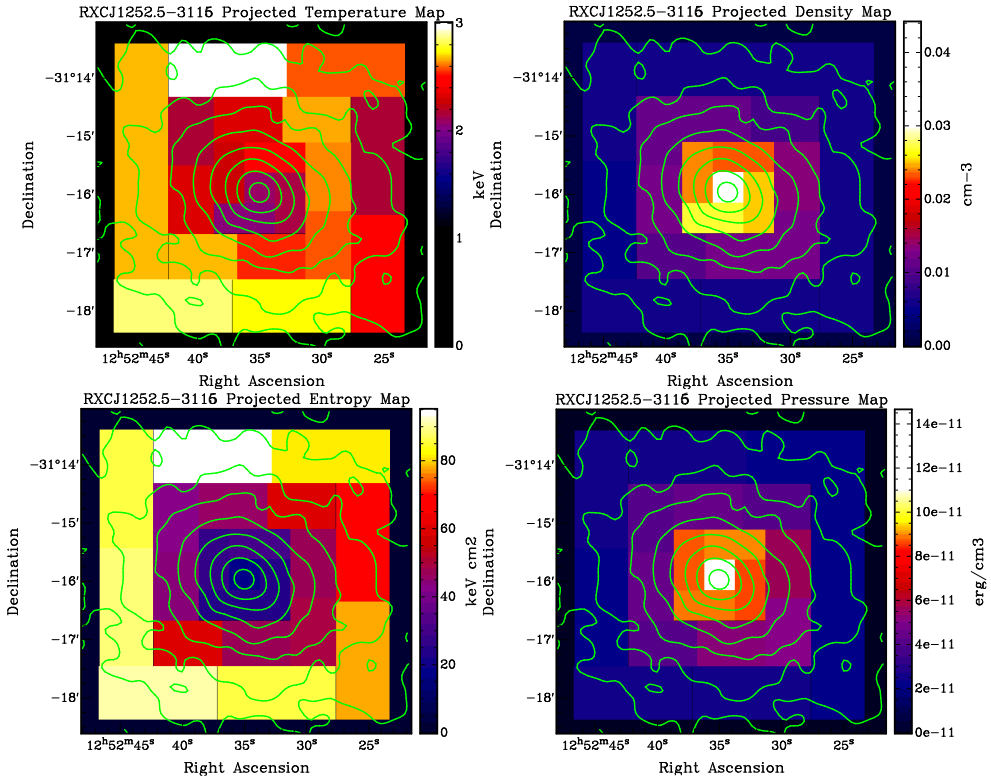

Figure 6. Projected maps of temperature (kT), electron density (n_e), entropy (S) and pressure (P) for the cluster RXC J1252.5–3116, obtained from the spectral analysis of box shaped regions (see §2.4). The overlaid green contours are from its *Chandra* image smoothed with a Gaussian kernel of width 8″ with intensity levels distributed from 3σ to 610σ above the mean background level.

the electron density (n_e), entropy (S), and pressure (P) are same as given in §2.3. The volume of each box was calculated using the relation given in Henry, Finoguenov & Briel (2004) and Ehlert et al. (2011). The resulting temperature (kT) maps are shown in Fig. 6; electron density (n_e) maps are shown in Fig. 6; entropy (S) maps are shown in Fig. 6; and pressure (P) maps are shown in Fig. 6. The temperature and entropy maps show low values at the centre. However, due to poor statistics and large errors in the outer parts the variations do not seem to be significant.

3. Summary

We have presented a detailed study of the cluster RXC J1252.5–3116 using its *Chandra* X-ray observation. X-ray emission of the cluster seems to be highly regular and symmetric (see Fig. 1) and extends to a distance of about 224″ (~0.22 Mpc) from the centre (significance > 3σ; see Fig. 2). In its optical image (Fig. 1), the BCG exactly coincides with the X-ray peak. The

Table 4. Estimates of 0.5-7.0 keV X-ray luminosity (L_X), bolometric X-ray luminosity (L_{bol}), cooling times (t_{cool}) and gas mass (M_{gas}(r)) (for r= 1 Mpc) for RXC J1252.5–3116.

L_X (0.5-7.0 keV) (10^{43} erg s^{-1})	L_X^{bol} (0.1-100 keV) (10^{43} erg s^{-1})	t_{cool} (10^9 yr)	M_{gas}(r = 1Mpc) (10^{12} $M_\odot$)
8.5 ± 0.1	11.3 ± 0.7	1.8 ± 0.3	9 ± 1

All errors are quoted at 90% confidence level based on χ^2_{min}+2.71.

cluster has a very low average X-ray temperature of 2.4±0.1 keV and an average elemental abundance of 0.5±0.1 times the solar value. RXC J1252.5–3116 shows near symmetric variations of temperature, entropy and pressure in its thermodynamic maps, although due to large errors the variations do not seem to be significant. Both projected and deprojected radial profiles of temperature (Fig. 6) suggest a possible decrease in the temperature inwards. The central cooling time of RXC J1252.5–3116 is equal to $0.18 \pm 0.03 \times 10^1 0$ yr, which is significantly lower than the Hubble time. RXC J1252.5–3116, therefore, seems to host a possible cool-core at its centre. The surface-brightness profiles of the cluster show a much better fit with a double-β model compared to the single-β model, indicating the presence of a double-phased central gas. In addition to this, the very small core radius of the small-core emission component of the double-β model, the very low values of the deprojected central temperature and entropy, and the high value of the classical mass deposition rate reinforce a possible cool core in the cluster.

Acknowledgements

The X-ray data used here have been obtained from the High Energy Astrophysics Science Archive Research Center (HEASARC), provided by NASA's Goddard Space Flight Center. We have used observations done with the *Chandra* X-ray Observatory, which is managed by NASA's Marshall -Center. This research has made use of data obtained from the SuperCOSMOS Science Archive, prepared and hosted by the Wide Field Astronomy Unit, Institute for Astronomy, University of Edinburgh, which is funded by the UK Science and Technology Facilities Council.

References

de Filippis E., Schindler S., Erben T., 2005, A&A, 444, 387.
Donnelly R. H., Forman W., Jones C., Quintana H., Ramirez A., Churazov E., Gilfanov M., 2001, ApJ, 562, 254
Eckert D., Molendi S., Paltani S., 2011, A&A, 526, A79
Ehlert S., et al., 2011, MNRAS, 411, 1641
Fabian A. C., 1994, ARA&A, 32, 277
Fabian A. C., 2012, ARA&A, 50, 455

Fukazawa Y., Ohashi T., Fabian A. C., Canizares C. R., Ikebe Y., Makishima K., Mushotzky R. F., Yamashita K., 1994, PASJ, 46, L55
Gu L.-Y., Wang Y., Gu J.-H., Wang J.-Y., Qin Z.-Z., Yao M.-Y., Yang J.-L., Xu H.-G., 2010, Research in Astronomy and Astrophysics, 10, 1005
Gu L., et al., 2012, ApJ, 749, 186
Henry J. P., Finoguenov A., Briel U. G., 2004, ApJ, 615, 181
Hudson D. S., Mittal R., Reiprich T. H., Nulsen P. E. J., Andernach H., Sarazin C. L., 2010, A&A, 513, A37
Kalberla P. M. W., Burton W. B., Hartmann D., Arnal E. M., Bajaja E., Morras R., Pöppel W. G. L., 2005, A&A, 440, 775
Lakhchaura K., Singh K. P., Saikia D. J., Hunstead R. W., 2011, ApJ, 743, 78
Lakhchaura K., Singh K. P., Saikia D. J., Hunstead R. W., 2013, ApJ, 767, 91
Morrison R., McCammon D., 1983, ApJ, 270, 119
Peres C. B., Fabian A. C., Edge A. C., Allen S. W., Johnstone R. M., White D. A., 1998, MNRAS, 298, 416
Pierre M., Boehringer H., Ebeling H., Voges W., Schuecker P., Cruddace R., MacGillivray H., 1994, A&A, 290, 725
Reid A. D., 2000, PASA, 17, 285
Smith R. K., Brickhouse N. S., Liedahl D. A., Raymond J. C., 2001, ApJL, 556, L91